

## New strategies for seismic attenuation at low frequency for third generation gravitational waves detectors(\*)

M. VACATELLO<sup>(1)(2)(\*\*)</sup>, S. ARDITO<sup>(1)(2)</sup>, M. BARATTI<sup>(1)(2)</sup>, G. BARTOLI<sup>(1)(2)</sup>,  
L. BELLIZZI<sup>(1)(2)</sup>, G. DEMASI<sup>(1)(3)</sup>, F. DE SANTI<sup>(1)(2)</sup>, F. FIDECARO<sup>(1)(2)</sup>,  
A. FIORI<sup>(1)(2)</sup>, L. MUCCILLO<sup>(1)(2)</sup>, M. A. PALAIA<sup>(1)(2)</sup>, L. PAPALINI<sup>(1)(2)</sup>  
and M. RAZZANO<sup>(1)(2)</sup>

<sup>(1)</sup> INFN, Sezione di Pisa - Pisa, Italy

<sup>(2)</sup> Dipartimento di Fisica, Università di Pisa - Pisa, Italy

<sup>(3)</sup> Dipartimento di Fisica, Università di Firenze - Firenze, Italy

received 2 December 2024

**Summary.** — Gravitational waves have revolutionised the way we study the Universe. The second-generation interferometers, LIGO, Virgo and KAGRA, are preparing for the next observational campaigns, while the future third-generation interferometers, Einstein Telescope and Cosmic Explorer, are expected to increase the sensitivity by an order of magnitude. In particular, improved low-frequency sensitivity is essential for detecting high-mass systems that allow to explore the Universe at high redshift, *i.e.*, before the formation of the first stars. Furthermore, good low-frequency sensitivity allows for better source localisation, effective pre-alerts for electromagnetic follow-up campaigns, and the detection of expected (but yet to be observed) gravitational waves emitted by sources such as rotating pulsars. In this proceeding, we will present ongoing experimental studies on new mechanical prototypes to address the low-frequency seismic noise attenuation.

### 1. – Introduction

The detection on September 14th 2015 of the first gravitational wave emitted by two coalescing black holes revolutionised our understanding of the universe [1]. Since then, multiple events have been observed in the first three observing runs, leading to a grand total of 90 official events [2-5]. The current operational detectors employed to find these elusive astrophysical phenomena are Advanced LIGO-Livingston, Advanced LIGO-Hanford [6], Advanced Virgo [7] and KAGRA [8]. They are modified L-shaped Michelson interferometers with km-long arms, enhanced with Fabry-Perot cavities to increase the

(\*) IFAE 2024 - “Cosmology and Astroparticles” session

(\*\*) E-mail: [michele.vacatello@phd.unipi.it](mailto:michele.vacatello@phd.unipi.it)

effective optical path of the circulating beam. The effect produced by gravitational waves on these detectors is of the order of  $\Delta L/L \sim 10^{-21}$ ,  $L$  being the arm of the interferometer. For what concerns the low frequency region (below 10 Hz), this translates to a physical displacement of  $\sim 10^{-18}$  m/ $\sqrt{\text{Hz}}$  at 10 Hz [9]. Since seismic noise is the dominant contribution to the total noise of the detectors in this low frequency region, it is crucial to reduce its impact. Many astrophysical sources of interest, such as high-redshift systems ( $z \gtrsim 30$ ) and isolated pulsars (20 – 200 Hz) [10], are foreseen to emit at low frequency. Improving the sensitivity in this region for the next generation of gravitational waves detectors will make it possible for such events to be detected. It will also make pre-alerts more effective for electromagnetic follow-up campaigns, since any signal will persist in the detectors sensitivity curve for a longer span of time (up to a few hours) [11].

## 2. – The Virgo Super Attenuator

**2.1. Seismic noise.** – At low frequencies, the main contribution to the noise of the detector is due to the seismic motion of the ground. The seismic noise can be divided in microseism ( $f < 1$  Hz), weather and wind ( $f \sim 1$  Hz) and anthropogenic activities ( $f \sim 10$  Hz). The empirical model [12] for its spectrum follows a power law of the form

$$(1) \quad \tilde{x}_{seism}(f) = A \left( \frac{1\text{Hz}}{f} \right)^2 \frac{\text{m}}{\sqrt{\text{Hz}}}$$

where  $A$  is a coefficient that depends on the specific site, but usually ranges between  $\sim 10^{-7} \div 10^{-9}$  (for the Advanced Virgo site in Cascina, Italy, we have  $A = 10^{-7}$  [13]). To meet the requirements on the residual motion of the mirrors, an attenuation of at least  $10^{11}$  is thus needed to filter the seismic noise.

**2.2. The pendulum chain.** – The mechanical system currently in charge of achieving the  $10^{11}$  required attenuation for Advanced Virgo is the Super Attenuator [9]. This passive system is composed of a preisolation stage consisting of an inverted pendulum, followed by a chain of five pendula in cascade. The whole system relies on the fact that the inverted pendulum and all the simple pendula behave as 2nd-order low-pass filters for frequencies much higher than their own resonance frequency. When we combine  $N$  pendula this way, we have for the total transfer function

$$(2) \quad T(\omega) = \prod_{i=1}^N \frac{1}{1 - (\omega/\omega_i)^2} \sim \frac{1}{\omega^{2N}}$$

for values of  $\omega$  much greater than all the resonance frequencies  $\omega_i$  of the system, that is  $\omega \gg \omega_i$  for all  $\omega_i$ . The horizontal modes of the 10 m high Virgo chain stand around  $\sim 0.5$  Hz to guarantee the proper attenuation above 10 Hz.

**2.3. The filters.** – The intermediate masses of the chain (called filters) are in charge of the vertical attenuation [9]. Being able to reduce the vertical noise is necessary because of the coupling between the horizontal and vertical directions due to the curvature of the Earth. They are drum-shaped steel filters with high inertia for damping the rotational modes (70 cm in diameter for 100 kg of mass), which are equipped with pre-bent elastic blades made of steel, ensuring the usual harmonic attenuation with a vertical resonance of  $\sim 1.4$  Hz. In order to have a response as isotropic as possible for the whole Super

Attenuator, the filters also host magnetic antisprings (made of magnets in a repulsive configuration) that allow to fine-tune the entire filter and make its vertical response less stiff. In this way, the vertical modes are lowered to a value of  $\sim 0.4$  Hz, similar to the horizontal modes of the chain.

### 3. – Shortening the pendulum chain

**3.1. The Pendulum Inverted Pendulum filter.** – The first detector of the 3rd generation, the Einstein Telescope, will be built underground at a depth of  $\sim 200 \div 300$  m [15]. The reference design for the suspensions of the core optics is a 17 m high Virgo-like Super Attenuator, which will need to be placed in dedicated caves. Developing a shorter suspension would significantly reduce the impact on the excavation costs and the personpower needed. The Pendulum Inverted Pendulum (PIP for short), is a new alternative design for a mechanical filter. The main idea is to apply the standard simple pendulum preattenuation followed by an inverted pendulum (see fig. 1), for every stage of the chain. This allows to essentially fold the Super Attenuator, and achieve twice the attenuation in the same height of a standard filter, thus reducing the overall height of the Super Attenuator. For the Sos Enattos mine in Sardinia, one of the candidate sites for the construction, a chain of 3 PIPs could meet the requirements for the residual seismic noise at 2 Hz, for a total height of about 4 m. We present here the preliminary studies we are conducting on the three inverted pendulum legs (the three, yellow vertical rods of fig. 1) that compose the PIP.

All position measurements have been performed with Linear Variable Differential Transformers (LVDTs) displacement sensors, placed at the bottom and the top of each

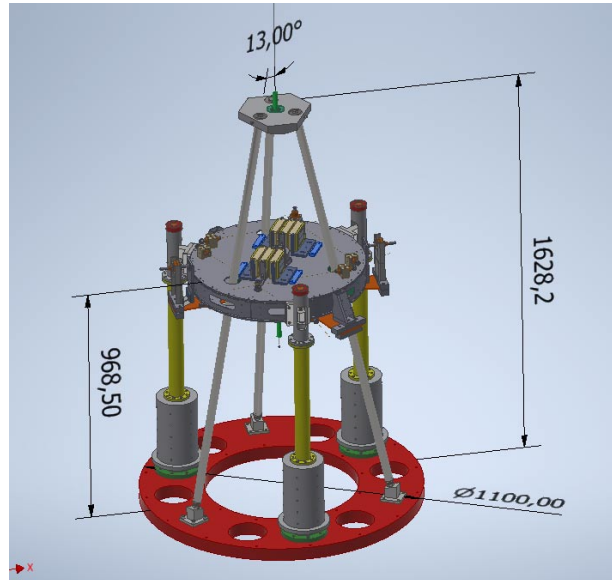


Fig. 1. – Technical design of the PIP. The wire at the top of the picture behaves as the simple pendulum. This is then connected through three metal rods to the bottom red ring, where the three yellow vertical legs make up the inverted pendulum. At the top of the inverted pendulum rests a Virgo-like filter, which is then connected through a wire to the next filter of the chain.

leg. Excitation signals were generated with 4  $V_{pp}$  sinusoidal sweeps between 100 mHz and 100 Hz with a MokuPro function generator. The signals were then fed to the mechanical system thanks to a woofer mounted at the base of the legs, to measure the displacement transfer function between the base and the top of each inverted pendulum.

**3.2. Top mass load effect.** – An inverted pendulum made of a rigid rod (mass  $m$ , length  $l$ , inertia  $I$ ) and stiffness  $k$ , linked to a top mass  $M$ , has a resonance frequency

$$(3) \quad \omega_0^2 = \frac{k - (M + m/2)g/l}{M + m/4 + I/l^2} = \frac{k - (M + m/2)g/l}{M + m/3}$$

where in the second equality we assume the rod to be uniform. This means that, by varying the top load  $M$ , an arbitrary low  $\omega_0$  can be in principle achieved. We measured different transfer functions (TF) for different loads to verify this behaviour, and fitted the resonance frequencies to find  $M_{0\text{Hz}}$ , the mass load for which the resonance frequency would theoretically become zero. The results are reported in figs. 2 and table I.

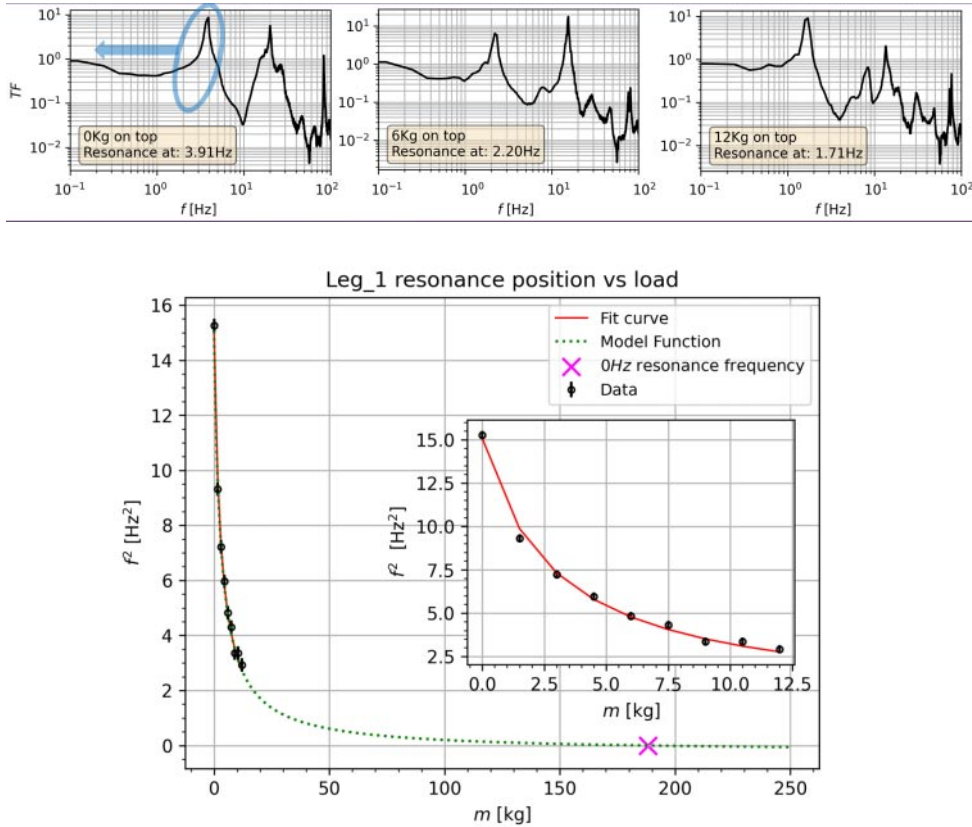


Fig. 2. – Top: shift of the resonance frequency *versus* the top load mass for the Leg.1 as seen in the transfer functions. Bottom: fit of the resonance frequencies with eq. (3).

TABLE I. – *Experimental results for the stiffness  $k$  and the critical mass  $M_{0Hz}$  for the three inverted pendulum legs.*

	Leg_1	Leg_2	Leg_3
$k$ [N/m]	1775	1816	1901
$M_{0Hz}$ [kg]	188	193	201

**3.3. Center of percussion effect.** – A real inverted pendulum has a non-zero mass rod, which introduces the so called center of percussion effect, represented by the quantity

$$(4) \quad \beta = \frac{m/4 - I/l^2}{M + m/4 + I/l^2}$$

This effect saturates the transfer function for  $\omega \gg \omega_0$ , so that there is a plateau instead of the usual  $1/\omega^2$  behaviour after the main resonance peak. By varying the inertia  $I$  of the system, we can make  $\beta$  as small as possible: this reduces the magnitude of the plateau and moves it at higher frequencies [14], where other sources of noise become the dominant contributors in the total noise of the detector. To investigate this, we have extra 4.7 kg weights that we can move along the inverted pendulum legs (at the base of the three legs in fig. 1) to fine-tune their inertia. We report in fig. 3 the preliminary study performed on the Leg\_1, which confirms that, for the first and second positions, we can indeed move the plateau at lower values. The results for the Leg\_2 and Leg\_3 show a similar behaviour.

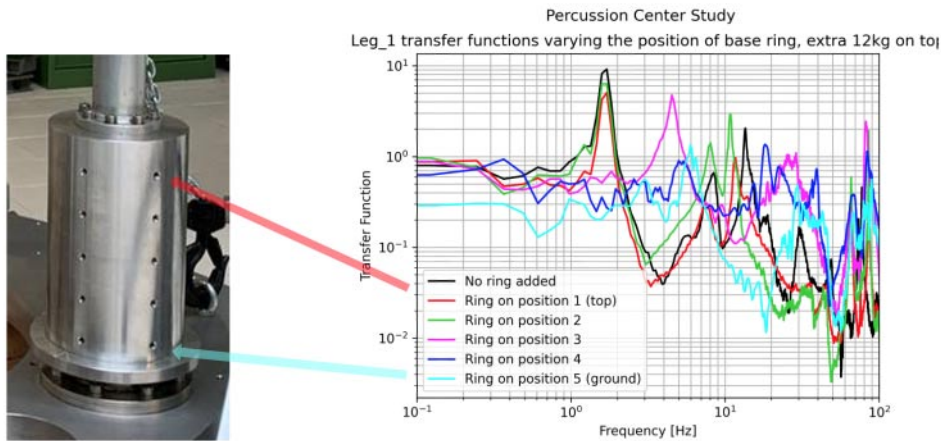


Fig. 3. – Left: base of one of the inverted pendulum legs. Right: different transfer functions according to different positions of the extra weights.

#### 4. – Conclusions

Here, we have presented the main idea behind the PIP concept and described the principal physical phenomena that can affect this system. We then characterised the inverted pendulum legs in a stand-alone configuration to better understand how the aforementioned effects manifest in the real prototype, confirming that the system behaves as expected and could be used for seismic isolation. We have now mounted the PIP in our laboratory and we will soon suspend it and start measurements to characterise how the whole prototype responds as a filter. We are starting simulations as well, which will allow for in-depth comparisons between predictions and the real prototype.

\* \* \*

The development of the PIP is supported by the MUR PRIN 20202C5XA9 project funded by the Italian Ministry of University and Research.

#### REFERENCES

- [1] ABBOTT B. P. *et al.*, *Phys. Rev. Lett.*, **116** (2016) 6.
- [2] ABBOTT B. P. *et al.*, *Phys. Rev. X*, **9** (2019) 3.
- [3] ABBOTT R. *et al.*, *Phys. Rev. X*, **11** (2021) 2.
- [4] ABBOTT R. *et al.*, arXiv:2108.01045 (2021).
- [5] ABBOTT R. *et al.*, *Phys. Rev. X*, **13** (2023) 4.
- [6] THE LIGO SCIENTIFIC COLLABORATION, *Class. Quantum Grav.*, **32** (2015) 7.
- [7] ACERNESE F. *et al.*, *Class. Quantum Grav.*, **32** (2015) 2.
- [8] THE KAGRA COLLABORATION, *Nat. Astron.*, **3** (2019) 35.
- [9] THE VIRGO COLLABORATION, Virgo Technical Documentation System, VIR-0128A-12 (2012).
- [10] MAGGIORE M. *et al.*, *J. Cosmol. Astropart. Phys.*, **03** (2020) 050.
- [11] RONCHINI S. *et al.*, *Astron. Astrophys.*, **665** (2022) A97.
- [12] SAULSON P. R., *Phys. Rev. D*, **30** (1984) 4.
- [13] TROZZO L., PhD Thesis (2018).
- [14] BOSCHI V., PhD Thesis (2010).
- [15] THE EINSTEIN TELESCOPE STEERING COMMITTEE, Einstein Telescope Documentation System, ET-0007A-20 (2020).